Journal of Information Hiding and Multimedia Signal Processing ©2017 ISSN 2073-4212
Ubiquitous International Volume **8**, Number **6**, November **2017**

Localized Sound Zone Generation Based on External Radiation Canceller

Takuma Okamoto

National Institute of Information and Communications Technology
3-5, Hikaridai, Seika-cho, Soraku-gun, Kyoto, 619-0289 Japan
okamoto@nict.go.jp

Received January 2017; revised June 2017

Abstract. *This paper provides two methods for realizing three-dimensional localized sound zone generation based on external radiation cancelling using multiple loudspeakers for personal sound systems. The radiation property produced by a spherical or circular loudspeaker array outside the sphere or the circle is different from that inside them. The sound pressure radiated from a spherical or circular array outside the sphere or the circle is completely canceled out using another point source or linear loudspeaker array. As a result, three-dimensional localized sound zone generation can be realized within their radii. Two methods, one based on external radiation cancelling using a spherical loudspeaker array and a point source, named ERC-SP, and the other using a circular and linear array combination, named ERC-CL, are proposed. The appropriate driving signals and the sound pressures produced by both methods are analytically derived. Compared with previous methods, the propagation distance can be controlled by changing their radii and these methods can be useful, not only in a free-field but also reverberant environments, because external radiations can be completely cancelled out. The results of computer simulations suggest that the proposed methods can create an effective localized sound zone in free-field and reverberant conditions.*
Keywords: Localized sound zone generation, external radiation, personal sound system, sound field synthesis, sound field control

1. **Introduction.** Generating a personalized listening area using multiple loudspeakers is receiving attention as an important and attractive sound media enrichment technique. A very well-known application is a personal sound system [1–8] that allows individual listening without headphones. In addition, multiple sound zones [7, 9–11] can simultaneously provide different sound signals at different positions to multi-users, which is useful for multilingual guide services without headsets. Furthermore, by combining image projection techniques, they can provide different audio-visual contents to different users and are also useful for virtual reality and multimedia applications.

To realize a personalized listening area, many approaches using multiple loudspeakers have been proposed, and are broadly categorized into two main approaches. The first, initially proposed in [12], controls the acoustic contrast or the energy between two spaces [2–5, 9–15]. In addition, an extended approach controls multiple sound fields [6–8, 16–20] so that they are simultaneously synthesized for different zones in space. These methods typically control sound areas away from the loudspeakers and a free-field is assumed in almost all the methods. However, the typical environments are reverberant and control accuracy is degraded by reverberation when these methods are applied in actual environments. In addition, although almost all the methods only consider two-dimensional control points

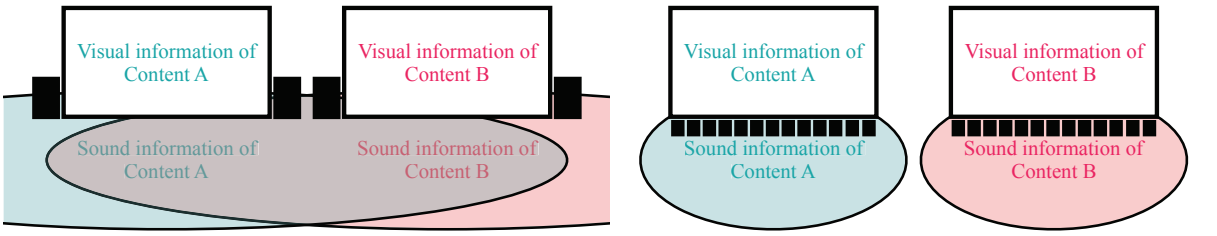

FIGURE 1. Comparison between (a) conventional multiple audio-visual systems and (b) multiple audio-visual systems with localized sound zone generation.

and their results are also two-dimensional [2, 4–6, 8–20], three-dimensional formulation and results are required for actual implementation [21].

In another approach, a localized sound zone is generated near loudspeakers so that audible sound pressure is only propagated close to them but at very low amplitudes beyond the reference distance. In this study, this approach is called localized sound zone generation, and may be suited to actual implementation, because sound pressure is not radiated at the walls and no reflections occur. In conventional audio-visual systems with simple loudspeakers, the sound contents are typically interfered each other (Fig. 1(a)). Those with localized sound zone generation, on the other hand, can only efficiently provide different audio-visual contents to different users in reverberant environments (Fig. 1(b)) since conventional multiple sound zone generation methods cannot be used in reverberant environments as discussed above. To investigate localized sound zone generation is, therefore, significant for the advancement of multimedia technology. The purpose of this study is then to develop methods for three-dimensional localized sound zone generation suitable for use in both free-field and reverberant environments.

Several methods for localized sound zone generation have been proposed. One is based on evanescent wave reproduction [22] using linear or circular arrays of loudspeakers [23, 24]. In this method, however, the attenuation property of the radiated sound cannot be controlled because the propagation property of an evanescent wave is dependent on the wave length [22]. Another method [25, 26], which uses double circular arrays, is based on least squares approaches [2–5, 12, 14, 16, 17]. However, such methods are quite unstable because the acoustic inverse problem is very ill-conditioned [22, 27]. To solve the ill-conditioned problem, an analytical approach using a circular double-layer array has been recently investigated [28]. In addition, an analytical method for localized sound zone generation based on sound source dimension mismatch with a linear loudspeaker array and a point source has been proposed [29]. However, these approaches are only considered in two-dimensional synthesis. The other methods [30,31] can synthesize a sound field only inside surrounding loudspeaker arrays and reduce the sound pressures propagated outside them which is called as external radiation. However, these methods require multiple spherical loudspeaker arrays [32] which can control complex directivities but are difficult to be implemented compared with simple loudspeakers.

To realize a three-dimensional localized sound zone generation in an actual environment and suitable for actual implementation, this paper proposes two methods. The primary concept of the proposal is that the sound pressure radiated from a spherical or circular loudspeaker array outside the sphere or the circle is completely canceled out using another point source or linear loudspeaker array. Adequate arrangements of both a spherical array and a point source are first proposed. The appropriate driving signals of the spherical loudspeaker array and the point source, and the sound pressures produced

by them are then analytically derived, based on spherical harmonic expansion [22]. This method is named the external radiation canceller using a spherical loudspeaker array and a point source, *ERC-SP*. In addition, to reduce the number of loudspeakers and actual implementation requirements, another method, which introduces circular and linear loudspeaker arrays instead of a spherical array and a point source, is proposed. This approach is named the external radiation canceller using a circular and linear loudspeaker array combination, *ERC-CL*. An adequate arrangement for both circular and linear arrays is proposed. The appropriate driving signals of the array, and the sound pressures produced by them are then also analytically derived based on the two-dimensional spatial Fourier transform [22].

The key point of both the proposed methods is that the radiation property produced by a spherical or circular loudspeaker array outside the sphere or circle is different from the radiation property inside them, and the external radiation can be perfectly canceled out and no reflection can occur in a reverberant environment. Compared with previous methods, three-dimensional formulations are introduced, the propagation distance can be controlled by changing the radius of a spherical or a circular array, the driving signals of both methods are based on analytical solutions instead of the least squares approach, and both proposed methods can be realized using multiple simple loudspeakers instead of multiple spherical loudspeaker arrays.

ERC-CL was partly presented in [33]. However, there are no detailed discussions about the sound pressure produced inside the circle, no comparisons with *ERC-SP*, and no simulations in reverberant conditions in [33].

The rest of this paper is organized as follows. Section 2 introduces the basic principles of the sound field resulting from continuous linear, cylindrical and spherical secondary monopole source distributions. Two methods for generating localized sound zones, *ERC-SP* using a spherical loudspeaker array and a point source, and *ERC-CL* using a circular and linear loudspeaker array combination are proposed in Section 3. In Section 4, computer simulations are conducted and the sound pressures produced by both methods are presented. Experimental results and the properties of both methods are compared and discussed in Section 5. Finally, conclusions are drawn in Section 6.

2. Sound field due to continuous linear, cylindrical and spherical secondary monopole source distributions.

To propose localized sound zone generation methods, the sound field produced by continuous linear, cylindrical and spherical secondary monopole source distributions instead of linear, cylindrical and spherical loudspeaker arrays are briefly introduced here for analytical formulations.

The sound pressure $P(\boldsymbol{x},\omega)$ synthesized at position $\boldsymbol{x} = [x,\ y,\ z]^{\mathrm{T}}$ by a continuous secondary source distribution is given as:

$$P(\boldsymbol{x},\omega) = \int_{dV_0} D(\boldsymbol{x}_0,\omega) G_{3\mathrm{D}}(\boldsymbol{x},\boldsymbol{x}_0,\omega) d\boldsymbol{x}_0, \tag{1}$$

where $\omega = 2\pi f$ denotes the radial frequency, f the temporal frequency, dV_0 the secondary source surface area, $D(\boldsymbol{x}_0,\omega)$ the secondary source driving function[1] at position $\boldsymbol{x}_0 = [x_0, y_0, z_0]^{\mathrm{T}}$, and $G_{3\mathrm{D}}(\boldsymbol{x},\boldsymbol{x}_0,\omega)$ the transfer function of the sound source placed at $\boldsymbol{x}_0$ to the point $\boldsymbol{x}$. Under the free-field assumption, $G_{3\mathrm{D}}(\boldsymbol{x},\boldsymbol{x}_0,\omega)$ is the three-dimensional free-field Green's function [22], defined as:

$$G_{3\mathrm{D}}(\boldsymbol{x},\boldsymbol{x}_0,\omega) = \frac{e^{-jk|\boldsymbol{x}-\boldsymbol{x}_0|}}{4\pi|\boldsymbol{x}-\boldsymbol{x}_0|}, \tag{2}$$

[1]Driving function instead of driving signal is used for continuous sound source distributions.

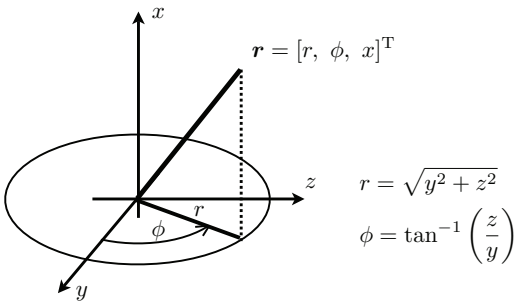

FIGURE 2. Definition of cylindrical coordinates $\boldsymbol{r} = [r,\ \theta,\ \phi]^{\mathrm{T}}$ relative to Cartesian coordinates $\boldsymbol{x} = [x,\ y,\ z]^{\mathrm{T}}$. for describing the sound field produced by linear, circular and cylindrical sound sources.

where $j = \sqrt{-1}$, $k = \omega/c$ denotes the wavenumber and c is the speed of sound [22].

2.1. **Continuous linear secondary source.** As in [11,21], the sound pressure produced by a continuous linear secondary monopole source distribution along the x-axis is given as:

$$P(\boldsymbol{x}, \omega) = \int_{-\infty}^{\infty} D(\boldsymbol{x}_0, \omega) G_{3\mathrm{D}}(\boldsymbol{x}, \boldsymbol{x}_0, \omega) dx_0. \tag{3}$$

The spatial Fourier transform of (3) with respect to x is then derived as:

$$\tilde{P}(r, k_x, \omega) = \tilde{D}(k_x, \omega) \tilde{G}(r, k_x, \omega), \tag{4}$$

where $\tilde{G}(r, k_x, \omega)$ is the transfer function in the wavenumber domain from linear sound source $r = 0$ to the produced cylinder r [36,37] and is given as:

$$\tilde{G}(r, k_x, \omega) = -\frac{j}{4} H_0^{(2)}\left(k_r r\right). \tag{5}$$

(4) is independent of ϕ and the sound pressure produced by a linear secondary source is radiated axisymmetrically to the x-axis.

2.2. **Continuous cylindrical secondary source.** To describe three-dimensional sound propagation using a continuous circular secondary monopole source distribution in the next section, the sound field produced by a continuous cylindrical secondary monopole source distribution is briefly introduced here.

Cylindrical coordinates $\boldsymbol{r} = [r,\ \phi,\ x]^{\mathrm{T}}$ relative to Cartesian coordinates $[x,\ y,\ z]^{\mathrm{T}}$ are defined in Fig. 2.

As in [33], the sound pressure $P(\boldsymbol{x}, \omega)$ synthesized at position $\boldsymbol{x} = [x,\ y,\ z]^{\mathrm{T}}$ by a continuous cylindrical secondary monopole source distribution with radius r_0 is also given as:

$$P(\boldsymbol{x}, \omega) = \int_0^{2\pi} \int_{-\infty}^{\infty} D(\boldsymbol{x}_0, \omega) G_{3\mathrm{D}}(\boldsymbol{x}, \boldsymbol{x}_0, \omega) r_0 dx_0 d\phi_0. \tag{6}$$

When applying the two-dimensional spatial Fourier transform [22] to (6) with respect to ϕ and x, their convolution is performed by the convolution theorem:

$$\tilde{P}_m(r, r_0, k_x, \omega) = 2\pi r_0 \tilde{D}_m(k_x, \omega) \tilde{G}_m(r, r_0, k_x, \omega), \tag{7}$$

where k_x denotes the spatial frequency in the direction of x. From [22,36], $\tilde{G}_m(r, r_0, k_x, \omega)$ is the two-dimensional spatial Fourier transform of $G_{3\mathrm{D}}(\boldsymbol{x}, \boldsymbol{x}_0, \omega)$ with respect to ϕ and x

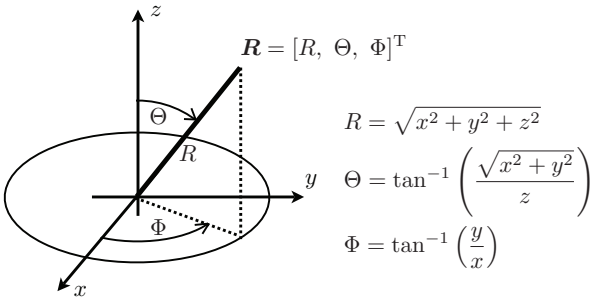

FIGURE 3. Definition of spherical coordinates $\boldsymbol{R} = [r,\ \theta,\ \phi]^{\mathrm{T}}$ relative to Cartesian coordinates $\boldsymbol{x} = [x,\ y,\ z]^{\mathrm{T}}$ for describing the sound field produced by a spherical sound source.

and is analytically derived as:

$$\tilde{G}_m(r_<, r_0, k_x, \omega) = -\frac{j}{4} J_m(k_r r) H_m^{(2)}(k_r r_0), \tag{8}$$

$$\tilde{G}_m(r_>, r_0, k_x, \omega) = -\frac{j}{4} J_m(k_r r_0) H_m^{(2)}(k_r r), \tag{9}$$

where $k_r = \sqrt{k^2 - k_x^2}$, $H_m^{(2)}$ and J_m denote the m-th order Hankel function of the second kind and the m-th order Bessel function of the first kind, respectively [22]. $\tilde{G}_m(r, r_0, k_x, \omega)$ is the transfer function in the herical wave spectrum domain from the sound source cylinder r_0 to the produced cylinder r.

From (7), (8) and (9), the sound pressures in the herical wave spectrum domain with $r < r_0$ and with $r > r_0$ are respectively derived as:

$$\begin{aligned}\tilde{P}_m(r_<, r_0, k_x, \omega) &= 2\pi r_0 \tilde{D}_m(k_x, \omega) \tilde{G}_m(r_<, r_0, k_x, \omega) \\ &= -\frac{j\pi r_0}{2} J_m(k_r r) H_m^{(2)}(k_r r_0) \tilde{D}_m(k_x, \omega),\end{aligned} \tag{10}$$

$$\begin{aligned}\tilde{P}_m(r_>, r_0, k_x, \omega) &= 2\pi r_0 \tilde{D}_m(k_x, \omega) \tilde{G}_m(r_>, r_0, k_x, \omega) \\ &= -\frac{j\pi r_0}{2} J_m(k_r r_0) H_m^{(2)}(k_r r) \tilde{D}_m(k_x, \omega).\end{aligned} \tag{11}$$

(10) and (11) suggest that the propagation property of a cylindrical secondary source with $r < r_0$ is different from that with $r > r_0$.

2.3. **Continuous spherical secondary source.** Spherical coordinates $\boldsymbol{R} = [R,\ \Theta,\ \Phi]^{\mathrm{T}}$ relative to Cartesian coordinates $\boldsymbol{x} = [x,\ y,\ z]^{\mathrm{T}}$ are defined in Fig. 3.

As in [34], the sound pressure $P(\boldsymbol{x}, \omega)$ synthesized at position $\boldsymbol{x} = [x,\ y,\ z]^{\mathrm{T}}$ by a continuous spherical secondary monopole source distribution with radius R_0 is given as:

$$P(\boldsymbol{x}, \omega) = \int_0^{2\pi} \int_0^{\pi} D(\boldsymbol{x}_0, \omega) G_{3\mathrm{D}}(\boldsymbol{x}, \boldsymbol{x}_0, \omega) R_0^2 \sin\Theta_0 d\Theta_0 d\Phi_0. \tag{12}$$

As in [38], the spherical convolution can be applied to (12) and their spherical harmonic expansion coefficients are derived as:

$$P_n^m(R, \omega) = R_0^2 \sqrt{\frac{4\pi}{2n+1}} D_n^m(R_0, \omega) G_n^0(R, R_0, \omega). \tag{13}$$

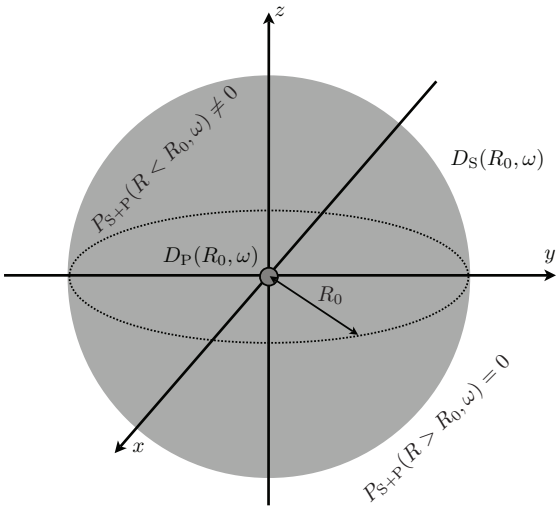

FIGURE 4. Proposed localized sound area generation method *ERC-SP* using the spherical source with radius R_0 and a point source centered origin. $D_{\mathrm{S}}(R_0, \omega)$ and $D_{\mathrm{P}}(R_0, \omega)$ are the driving functions of the spherical and point sound sources analytically derived in (18) and (23). The produced sound pressures $P_{\mathrm{S+P}}(R, R_0, \omega)$ for $R > R_0$ and $R < R_0$ are analytically calculated using (24) and (25).

From [22] and [38], $G_n^0(R, R_0, \omega)$ for $R < R_0$ and $R > R_0$ are respectively given as:

$$G_n^0(R_<, R_0, \omega) = -jk\sqrt{\frac{2n+1}{4\pi}} j_n(kR) h_n^{(2)}(kR_0), \tag{14}$$

$$G_n^0(R_>, R_0, \omega) = -jk\sqrt{\frac{2n+1}{4\pi}} j_n(kR_0) h_n^{(2)}(kR), \tag{15}$$

where j_n is the n-th order spherical Bessel function, $h_n^{(2)}$ is the n-the order spherical Hankel function of the second kind, respectively [22].

From (13), (14) and (15), the sound pressures in the spherical harmonic domain with $R < R_0$ and with $R > R_0$ are respectively derived as:

$$P_n^m(R_<, R_0, \omega) = -jkR_0^2 D_n^m(R_0, \omega) j_n(kR) h_n^{(2)}(kR_0), \tag{16}$$

$$P_n^m(R_>, R_0, \omega) = -jkR_0^2 D_n^m(R_0, \omega) j_n(kR_0) h_n^{(2)}(kR). \tag{17}$$

(16) and (17) indicate that the propagation property of a spherical secondary source with $R < R_0$ is also different from that with $R > R_0$.

3. Localized sound zone generation based on an external radiation canceller using two types of sound sources.

In this section, two methods for generating a localized sound zone based on external radiation cancelling are proposed. As described in Sec. 2, the radiation property produced by a spherical or circular sound source outside the sphere or circle is different from the radiation property inside them, and the external radiation can be perfectly canceled out using another point or linear sound source in the proposed methods.

3.1. ERC-SP: using spherical and point sound sources.

A localized sound zone generation method based on external radiation cancelling using a spherical and point source combination, named *ERC-SP*, is proposed here. In *ERC-SP*, the sound pressure

radiated from a spherical sound source outside the sphere is completely canceled out by a point source at the center of the sphere. To realize this situation, a spherical sound source with radius R_0 and a point source are centered on the origin as shown in Fig. 4.

It is obvious that the sound pressure produced by a point source $P_{\mathrm{P}}(\boldsymbol{x}, \omega)$ is omnidirectionally radiated. To cancel external radiation from a spherical sound source using a point source, the sound pressure synthesized by a spherical sound source $P_{\mathrm{S}}(\boldsymbol{x}, \omega)$ must also be omnidirectionally radiated and $P_{\mathrm{S}}(\boldsymbol{x}, \omega)$ is independent of Θ and Φ $(= P_{\mathrm{S}}(R, \omega))$. The driving function of a spherical sound source must then also be independent of Θ and Φ and is given as:

$$D_{\mathrm{S}}(R_0, \omega) = D^0_{0,\mathrm{S}}(R_0, \omega) = \frac{S(\omega)}{4\pi R_0^2}, \tag{18}$$

where $S(\omega)$ is the sound source signal in the time-frequency domain and $D_{\mathrm{S}}(R_0, \omega)$ is normalized by the superficial area of a spherical sound source $4\pi R_0^2$. It follows that the spherical harmonic expansions of $P_{\mathrm{S}}(\boldsymbol{x}, \omega)$ and $D_{\mathrm{S}}(R_0, \omega)$ have only the 0-th order component.

From (16) and (18), the sound pressure produced by an omnidirectional spherical sound source with $R < R_0$ is analytically derived as:

$$P_{\mathrm{S}}(R_<, R_0, \omega) = P^0_{0,\mathrm{S}}(R_<, R_0, \omega) = j_0(kR)\frac{e^{-jkR_0}}{4\pi R_0} S(\omega), \tag{19}$$

and from (17) and (18), that with $R > R_0$ is also analytically derived as:

$$P_{\mathrm{S}}(R_>, R_0, \omega) = P^0_{0,\mathrm{S}}(R_>, R_0, \omega) = j_0(kR_0)\frac{e^{-jkR}}{4\pi R} S(\omega), \tag{20}$$

where $-jkh_0^{(2)}(kR) = e^{-jkR}/R$ [22].

To cancel out external radiation from a spherical sound source $P_{\mathrm{S}}(R_>, R_0, \omega)$ by a point source, the appropriate driving function of a point source $D_{\mathrm{P}}(\omega)$ is analytically derived. The sound pressure produced by a point source is given as:

$$P_{\mathrm{P}}(R, \omega) = D_{\mathrm{P}}(\omega)\frac{e^{-jkR}}{4\pi R}. \tag{21}$$

For cancelling $P_{\mathrm{S}}(R_>, R_0, \omega)$,

$$P_{\mathrm{P}}(r, \omega) = -P_{\mathrm{S}}(R_>, R_0, \omega) = -j_0(kR_0)\frac{e^{-jkR}}{4\pi R} S(\omega). \tag{22}$$

Then, from (21) and (22),

$$D_{\mathrm{P}}(R_0, \omega) = -j_0(kR_0) S(\omega). \tag{23}$$

Finally, from (20) and (22), the total sound pressure produced by both the spherical and point sources for $R > R_0$ is completely canceled out as:

$$P_{\mathrm{S+P}}(R_>, R_0, \omega) = P_{\mathrm{S}}(R_>, R_0, \omega) + P_{\mathrm{P}}(R, \omega) = 0. \tag{24}$$

However, the sound pressure produced for $R < R_0$ is obtained from (19) and (22) as:

$$\begin{aligned} P_{\mathrm{S+P}}(R_<, R_0, \omega) &= P_{\mathrm{S}}(R_<, R_0, \omega) + P_{\mathrm{P}}(R, \omega) \\ &= S(\omega)\left\{ j_0(kR)\frac{e^{-jkR_0}}{4\pi R_0} - j_0(kR_0)\frac{e^{-jkR}}{4\pi R} \right\} \\ &= -\frac{jkS(\omega)}{4\pi}\left\{ j_0(kR)h_0^{(2)}(kR_0) - j_0(kR_0)h_0^{(2)}(kR) \right\}. \end{aligned} \tag{25}$$

As a result, (24) and (25) suggest that the *ERC-SP* can generate a three-dimensional localized sound zone within $R < R_0$.

For making the sound pressure radiated from a point source penetrate to $R > R_0$ and actual implementation, a continuous spherical sound source must be discretized as a spherical array of loudspeakers. When the channel number of a spherical array of loudspeakers is N_{S}, (12) is discretized as:

$$\begin{aligned} P(\boldsymbol{x},\omega) &\approx \sum_{i=1}^{N_{\mathrm{S}}} \frac{4\pi R_0^2}{N_{\mathrm{S}}} D_{\mathrm{S}}(\boldsymbol{x}_i,\omega) G_{\mathrm{3D}}(\boldsymbol{x},\boldsymbol{x}_i,\omega) \\ &= \sum_{i=1}^{N_{\mathrm{S}}} D_{\mathrm{S},i}(\omega) G_{\mathrm{3D}}(\boldsymbol{x},\boldsymbol{x}_i,\omega), \end{aligned} \tag{26}$$

where $D_{\mathrm{S},i}(\omega) = S(\omega)/N_{\mathrm{S}}$ defines the discretized driving signals of a spherical array of loudspeakers.

When $D_{\mathrm{S},i}(\omega)$ and (23) are divided by $-j_0(kR_0)$, the coefficients of the driving signals of a spherical array of loudspeakers and a loudspeaker on the origin, are simply equivalent to those of a close-talking microphone array using a spherical array of microphones and a microphone at the center [39]. It is thought-provoking that the coefficients for [39] are derived from the interpolation of sound pressure based on a spherical harmonic expansion [22] and a different approach from *ERC-SP*, but the final coefficients are equivalent to the *ERC-SP*. In [39], the reason close-talking can be realized is explained noting that if the sound source is close to the spherical array, the array cannot express the spherical waves correctly because the number of microphones is limited and the sound source signal can be obtained from the residual signal. From the point of view of the acoustical principle of reciprocity, the principle of a close-talking microphone array can also be explained by the fact that this array can make nulls at $R > R_0$ shown in (24) derived by *ERC-SP*.

3.2. **ERC-CL: Using circular and linear sound sources.** Although *ERC-SP* can completely cancel out external radiation and generate a localized sound zone theoretically, there is a problem in its realistic implementation. *ERC-SP* requires a large number of loudspeakers when controlling a large area in which there are listeners. To reduce the number of loudspeakers, another method using circular and linear sound sources, named *ERC-CP*, is proposed.

In *ERC-CP*, the sound pressure radiating from a circular sound source outside the circle is also completely canceled out by a linear source. A continuous circular sound source with radius r_0 is centered at the origin on the y-z plane and a continuous linear sound source is located along the x-axis as shown in Fig. 5. This situation can also be realized with cylindrical and linear sources. However, for realistic implementation, the number of loudspeakers should be reduced, and the proposed method introduces a circular source instead of a cylindrical source.

As shown in (4), the sound pressure produced by a linear sound source $P_{\mathrm{L}}(\boldsymbol{r},\omega)$ is radiated axisymmetrically to the x-axis. The sound pressure produced by a circular sound source $P_{\mathrm{C}}(\boldsymbol{r},\omega)$ must then also be radiated axisymmetrically to the x-axis. It is apparent that $\tilde{P}_{\mathrm{C},n}(r,k_x,\omega)$ only has a 0-th order component ($n = 0$), and the driving function of a circular source is then independent of ϕ and given as:

$$\begin{aligned} D_{\mathrm{C}}(r_0,\omega) &= \begin{cases} S(\omega)/2\pi r_0 & \text{for } x = 0 \\ 0 & \text{for } x \neq 0 \end{cases} \\ &= \frac{S(\omega)\delta(x)}{2\pi r_0}, \end{aligned} \tag{27}$$

where $\delta(x)$ is a delta function [22] and $D_{\mathrm{C}}(r_0,\omega)$ is also normalized by the circumference of a circular sound source $2\pi r_0$.

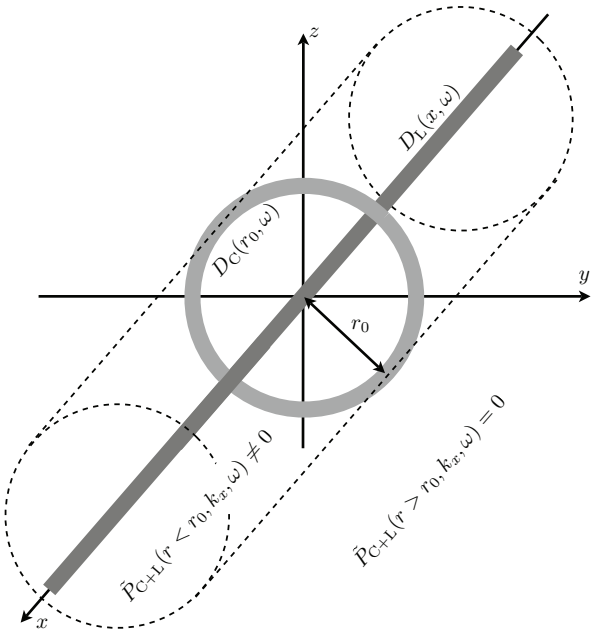

FIGURE 5. Proposed localized sound area generation method *ERC-CL* using a circular sound source with radius r_0 centered at the origin on the y-z plane and a linear sound source along the x-axis. $D_{\mathrm{C}}(r_0,\omega)$ and $D_{\mathrm{L}}(x,\omega)$ are the driving functions of the circular and linear sound sources analytically derived in (27) and (37). The produced sound pressures $\tilde{P}_{\mathrm{C+L}}(r,k_x,\omega)$ for $r>r_0$ and $r<r_0$ are analytically calculated using (38) and (39).

The driving function of a circular source in the helical wave spectrum domain with $n=0$ is calculated from the spatial Fourier transform to (27) with respect to x and is obtained as:

$$\tilde{D}_{0,\mathrm{C}}(k_x,\omega)=\int_{-\infty}^{\infty}D_{\mathrm{C}}(r_0,\omega)e^{-jk_xx}dx=\frac{S(\omega)}{2\pi r_0}. \tag{28}$$

From (10), (11), and (28), the sound pressure produced by a circular source in the helical wave spectrum domain with $n=0$ is analytically derived as:

$$\tilde{P}_{0,\mathrm{C}}(r_<,r_0,k_x,\omega)=-\frac{j}{4}J_0(k_rr)H_0^{(2)}(k_rr_0)S(\omega), \tag{29}$$

$$\tilde{P}_{0,\mathrm{C}}(r_>,r_0,k_x,\omega)=-\frac{j}{4}J_0(k_rr_0)H_0^{(2)}(k_rr)S(\omega). \tag{30}$$

ERC-CL also suggests that the propagation property of a circular source for $r<r_0$ is different from that for $r>r_0$. $\tilde{P}_{0,\mathrm{C}}(r,k_x,\omega)$ is obviously equivalent to the spatial Fourier transform coefficient $\tilde{P}_{\mathrm{C}}(r,k_x,\omega)$ with respect to x and describes the three-dimensional sound propagation produced by a circular source.

The driving function of a linear sound source $D_{\mathrm{L}}(x,\omega)$, which is appropriate for canceling out $\tilde{P}_{0,\mathrm{C}}(r>r_0,k_x,\omega)$ in (30), is analytically derived. From (4), the sound pressure resulting from a linear source along the x-axis in the wavenumber domain $\tilde{P}_{\mathrm{L}}(r,k_x,\omega)$ is given as:

$$\tilde{P}_{\mathrm{L}}(r,k_x,\omega)=\tilde{D}_{\mathrm{L}}(k_x,\omega)\tilde{G}(r,k_x,\omega), \tag{31}$$

To cancel $\tilde{P}_{0,\mathrm{C}}(r_>,r_0,k_x,\omega)$ in (30) by $\tilde{D}_{\mathrm{L}}(k_x,\omega)$,

$$\tilde{P}_{\mathrm{L}}(r,k_x,\omega)=-\tilde{P}_{0,\mathrm{C}}(r_>,r_0,k_x,\omega), \tag{32}$$

and from (5), (31) and (32), $\tilde{D}_{\mathrm{L}}(k_x,\omega)$ can be analytically derived by the spectral division method [37] as:

$$\tilde{D}_{\mathrm{L}}(k_x,\omega)=\frac{-\tilde{P}_{0,\mathrm{C}}(r_>,r_0,k_x,\omega)}{\tilde{G}(r,k_x,\omega)}=-J_0(k_r r_0)S(\omega). \tag{33}$$

Compared with 2.5D sound field synthesis [9–11, 28, 37, 40, 41], it is important that $\tilde{D}_{\mathrm{L}}(k_x,\omega)$ is independent of r and:

$$\tilde{P}_{\mathrm{L}}(r,k_x,\omega)=\frac{j}{4}H_0^{(2)}\left(k_r r\right)J_0\left(k_r r_0\right), \tag{34}$$

can be completely produced.

Finally, from (30) and (34), the total sound pressure produced by both the circular and linear sources for $r>r_0$ is completely canceled out for all r_0 and k_x

$$\tilde{P}_{\mathrm{C+L}}(r_>,r_0,k_x,\omega)=\tilde{P}_{0,\mathrm{C}}(r_>,r_0,k_x,\omega)+\tilde{P}_{\mathrm{L}}(r,k_x,\omega)=0. \tag{35}$$

The sound pressure produced for $r<r_0$, however, is calculated from (29) and (34) as:

$$\begin{aligned}\tilde{P}_{\mathrm{C+L}}(r_<,r_0,k_x,\omega)&=\tilde{P}_{0,\mathrm{C}}(r_<,r_0,k_x,\omega)+\tilde{P}_{\mathrm{L}}(r,k_x,\omega)\\&=-\frac{j}{4}S(\omega)\left\{J_0(k_r r)H_0^{(2)}(k_r r_0)-J_0(k_r r_0)H_0^{(2)}(k_r r)\right\}.\end{aligned} \tag{36}$$

As a result, (35) and (36) suggest that the *ERC-CL* can realize three-dimensional localized sound area generation within $r<r_0$ and the propagation distance can be controlled by changing the radius of the circular source r_0.

To calculate stable driving signals, $\tilde{D}_{\mathrm{L}}(k_x,\omega)=0$ for $k_r^2=k^2-k_x^2\le 0$, corresponding to the evanescent wave components [11,21]. The inverse spatial Fourier transform of (33) is then analytically calculated from (41) in the Appendix and given as:

$$D_{\mathrm{L}}(x,\omega)=-\frac{S(\omega)}{\pi}\cdot\frac{\sin\left(k\sqrt{x^2+r_0^2}\right)}{\sqrt{x^2+r_0^2}}\qquad\text{for } |k|>|k_x|. \tag{37}$$

In this case, the propagation wave components radiated by a circular sound source only are cancelled out and (35) is represented as:

$$\tilde{P}_{\mathrm{C+L}}(r_>,r_0,k_x,\omega)=\begin{cases}0 & \text{for } |k|>|k_x|\\ -\frac{j}{4}S(\omega)j_0(k_r r_0)H_0^{(2)}(k_r r) & \text{for } |k|\le|k_x|\end{cases}, \tag{38}$$

and (36) is also represented as:

$$\tilde{P}_{\mathrm{C+L}}(r_<,r_0,k_x,\omega)=\begin{cases}-\frac{j}{4}S(\omega)\left\{J_0(k_r r)H_0^{(2)}(k_r r_0)-J_0(k_r r_0)H_0^{(2)}(k_r r)\right\} & \\ \qquad\qquad\qquad\qquad\text{for } |k|>|k_x| & ,\\ -\frac{j}{4}S(\omega)j_0(k_r r)H_0^{(2)}(k_r r_0) & \\ \qquad\qquad\qquad\qquad\text{for } |k|\le|k_x| & \end{cases} \tag{39}$$

In a practical implementation, a circular and a linear array of loudspeakers is used instead of continuous circular and linear sound sources. (27) and (37) must then be discretized and (37) must be truncated.

3.3. **Spatio-temporal forbidden frequencies.** In sound field control outside the array using a spherical or a circular array of loudspeakers [10, 35], temporal forbidden frequencies [22] corresponding to $h_n^{(2)}(kR_0)=0$ or $H_n^{(2)}(kr_0)=0$, dependent on the radius of the array, are a problem, and their sound field is out of control. To control their sound field, a rigid sphere or a rigid cylinder is introduced [10, 35]. In contrast, both proposed methods theoretically employ an open spherical or an open circular array of loudspeakers. However, (24), (25), (38) and (39) in both the proposed methods hold,

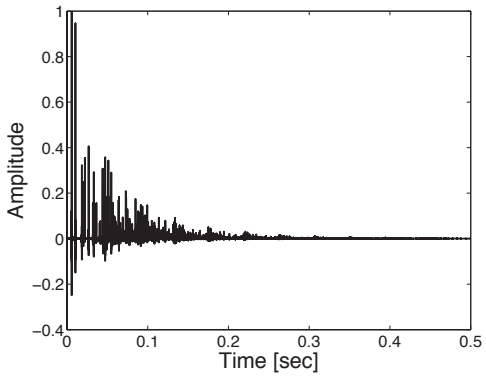

FIGURE 6. Impulse response between a monopole at the origin and received point at $\boldsymbol{x} = [0,\ 2,\ 0]^{\mathrm{T}}$ simulated using the image method. The rectangular room was $[15,\ 9,\ 3]^{\mathrm{T}}$, reflection coefficient 0.75, number of reflection times 10 and reverberation time about 569 ms.

and (25) and (39) are not 0 even though $h_0^{(2)}(kR_0) = 0$ and $H_0^{(2)}(k_r r_0) = 0$. Therefore, the temporal forbidden frequencies corresponding to $h_0^{(2)}(kR_0) = 0$ or $H_0^{(2)}(k_r r_0) = 0$ are not a problem in both proposed methods. Meanwhile, both proposed methods have other spatio-temporal forbidden frequencies corresponding to when (25) and (39) are 0, where $j_0(kR)h_0^{(2)}(kR_0) = j_0(kR_0)h_0^{(2)}(kR)$, dependent on k, R_0 and R in *ERC-SP* and $J_0(k_r r)H_0^{(2)}(k_r r_0) = J_0(k_r r_0)H_0^{(2)}(k_r r)$, dependent on k, k_x, r_0 and r in *ERC-CL*.

4. Experiments.

4.1. **Experimental conditions.** Computer simulations were conducted to evaluate both proposed methods. In all the calculations, the speed of sound c is 343.26 m/s and the sound source signal $S(\omega) = 1$. The channel numbers of the spherical array for *ERC-SP*, the circular and linear arrays for *ERC-CL* were $N_{\mathrm{S}} = 162$, $N_{\mathrm{C}} = 32$ and $N_{\mathrm{L}} = 64$, respectively. The arrangement of the spherical array of 162 loudspeakers was calculated using the subdivision method [42] and nearly equidensity on a spherical surface. The distance between adjacent loudspeakers of the linear array was $\Delta x = 0.05$ m. For evaluating not only in three-dimensional free-field condition but also in a reverberant condition, the reflections from the walls were simulated using the image method [43]. A rectangular room $[15,\ 9,\ 3]^{\mathrm{T}}$ was assumed, the reflection coefficient was 0.75 and the number of reflection times was 10. In the reverberant condition, each array was set at the center of the room. The simulated impulse response between a monopole sound source at the origin and the received point at $\boldsymbol{x} = [0,\ 2,\ 0]^{\mathrm{T}}$ is shown in Fig. 6. The reverberation time of the simulated room is about 569 ms.

4.2. **Results.** Figs. 7(a-1) to (c-2) show the results of the sound pressures produced by a circular array, a linear array and both arrays, respectively. The radius of the circular array was $r_0 = 0.25$ m, and $f = 3$ kHz. Figs. 7(d-1) and (d-2) show the sound pressure level of the produced sound pressure in Figs. 7(c-1) and (c-2). The results in Figs. 7(a-1) to (c-2) suggest that the propagated sound pressure by a circular array $P_{\mathrm{C}}(\boldsymbol{r}, \omega)$ for $r > r_0$ is produced by a linear array with an antiphase of $P_{\mathrm{L}}(\boldsymbol{r}, \omega)$, and the total sound pressure produced can be efficiently canceled for $r > r_0$. Moreover, the results of Figs. 7(d-1) and (d-2) indicate that a localized sound zone can be generated at $r < r_0$ not only for the free-field but also in a reverberant environment.

The results of the sound pressure level of the total sound produced by both proposed methods for $f = 1$ kHz in the free-field and reverberant conditions are depicted in

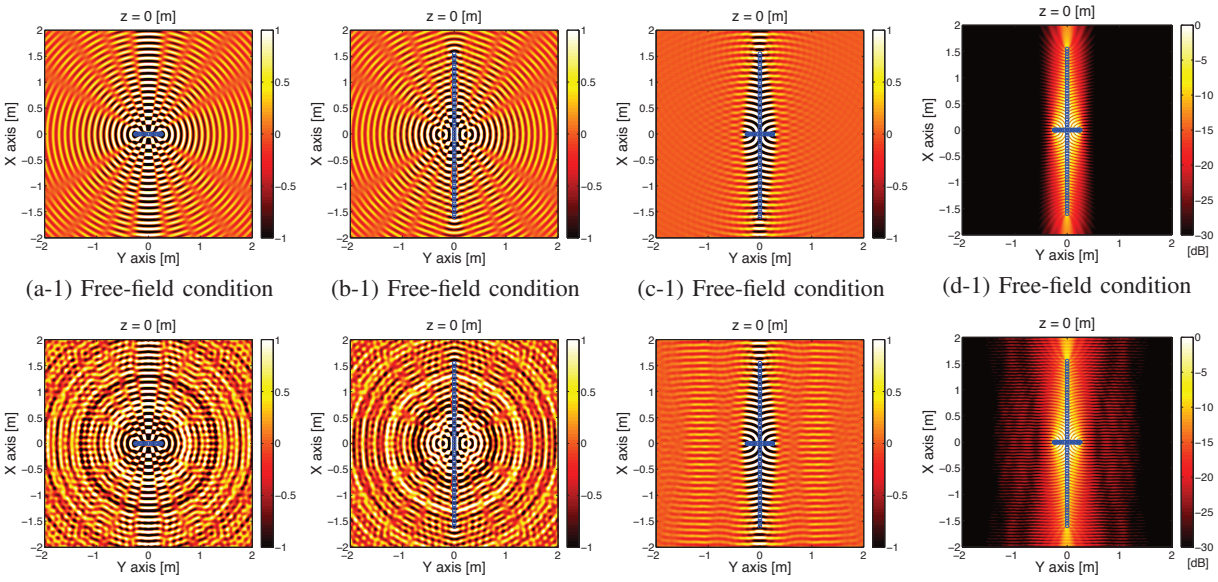

(a-1) Free-field condition (b-1) Free-field condition (c-1) Free-field condition (d-1) Free-field condition

(a-2) Reverberant condition (b-2) Reverberant condition (c-2) Reverberant condition (d-2) Reverberant condition

$\Re\{P_{\mathrm{C}}(\boldsymbol{r},\omega)\}$ $\Re\{P_{\mathrm{L}}(\boldsymbol{r},\omega)\}$ $\Re\{P_{\mathrm{C+L}}(\boldsymbol{r},\omega)\}$ $20\log_{10}|P_{\mathrm{C+L}}(\boldsymbol{r},\omega)|$

FIGURE 7. Results of (a)-(c) produced sound pressure and (d) sound pressure level by *ERC-CL* with the radius of the circular array $r_0 = 0.25$ m for $f = 3$ kHz in (1) the free-field condition and (2) the reverberant condition. $\Re\{\cdot\}$ denotes the real part of the complex number. Blue circles are loudspeakers. Channel numbers of the circular and linear arrays are $N_{\mathrm{C}} = 32$ and $N_{\mathrm{L}} = 64$. Distance between adjacent loudspeakers in the linear array is $\Delta x = 0.05$ m. Sound pressure level at $\boldsymbol{x} = [0,\ 0.1,\ 0]^{\mathrm{T}}$ is set to 0 dB in (d).

Figs. 8(b-1) and (b-2) for *ERC-SP* with $R_0 = 0.8$ m and Figs. 8(c-1) to (d-2) for *ERC-CL* with $r_0 = 0.25$ m and 0.4 m, respectively. The maximum distance between adjacent loudspeakers of the spherical array in Figs. 8(b-1) and (b-2) was about 0.26 m and the spatial Nyquist of *ERC-SP* in Figs. 8(b-1) and (b-2) was about 660 Hz. That of the *ERC-CL* in Figs. 8(c-1) and (c-2) with $r_0 = 0.25$ and in Figs. 8(d-1) and (d-2) with $r_0 = 0.4$ was about 3.4 and 2.2 kHz, respectively.

In addition, the sound pressure level produced by *ERC-SP* with $R_0 = 0.25$ m at $x = 0$ m and that of *ERC-SP* with $r_0 = 0.25$ m and at $x = 0$ and 1 m for $0.01 < f < 5$ kHz is plotted in Figs. 9(b-1) to (d-2), respectively. The spatial Nyquist frequency of *ERC-SP* in Figs. 9(b-1) and (b-2) was about 2.1 kHz and that of *ERC-CL* in Figs. 9(c-1) to (d-2) was also about 3.4 kHz

These results are compared with those of a monopole point source respectively shown in Figs. 8(a-1), (a-2) and 9(a-1) (a-2).

Throughout the experiments, the results of Figs. 8 and 9 suggest that both *ERC-SP* and *ERC-CL* can generate localized sound zones within $R < R_0$ and $r < r_0$ effectively, relative to a monopole sound source not only in a free-field but also in a reverberant condition. Moreover, the results in Fig. 8(c-1) and (c-2) for $r_0 = 0.25$ m and in Fig. 8(d-1) and (d-2) for $r_0 = 0.4$ m indicate that the propagation distance can be controlled by changing the radius of a circular array.

5. **Discussion.**

In this section, the proposed methods are evaluated using the experimental results. In addition, extended work on actual implementations are discussed.

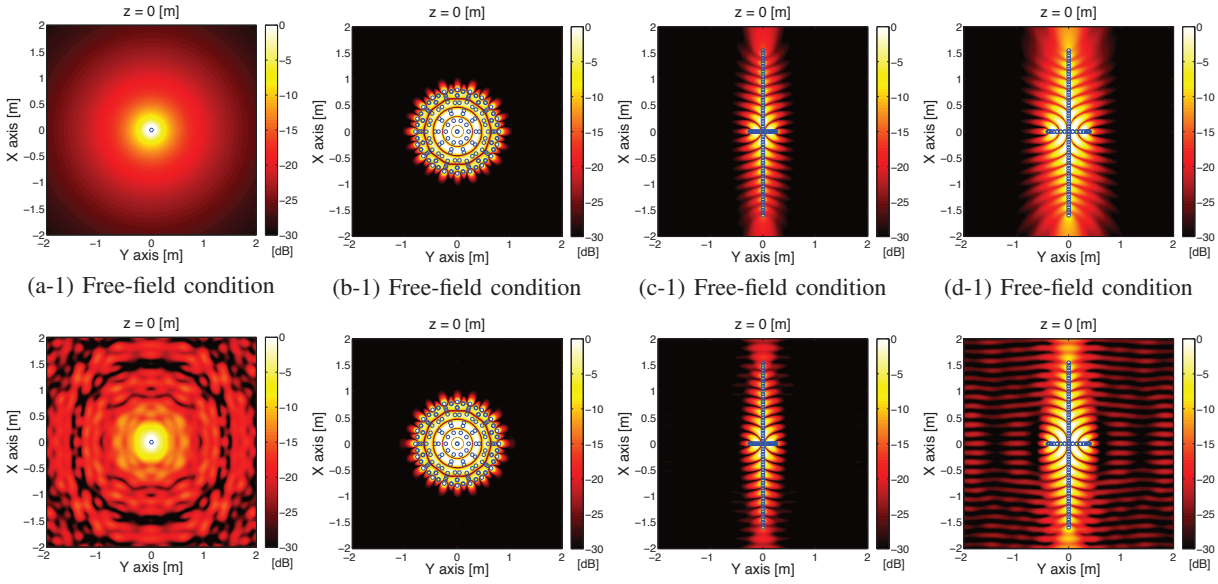

(a-1) Free-field condition (b-1) Free-field condition (c-1) Free-field condition (d-1) Free-field condition

(a-2) Reverberant condition (b-2) Reverberant condition (c-2) Reverberant condition (d-2) Reverberant condition

Monopole *ERC-SP* R_0 =0.8 m *ERC-CL* r_0 =0.25 m *ERC-CL* r_0 =0.4 m

FIGURE 8. Results of sound pressure level $20\log_{10}|P(\boldsymbol{x},\omega)|$ produced by (a) monopole point source, (b) *ERC-SP* with $N_{\mathrm{S}} = 162$ and (c)-(d) *ERC-CL* with $N_{\mathrm{C}} = 32$, $N_{\mathrm{L}} = 64$, and $\Delta x = 0.05$ m for $f = 1$ kHz in (1) the free-field condition and (2) the reverberant condition. Blue circles are loudspeakers. Sound pressure level at $\boldsymbol{x} = [0,\ 0.1,\ 0]^{\mathrm{T}}$ is set to 0 dB.

From the results of Figs. 8(b-1) and 9(b-1), *ERC-SP* perfectly cancels out external radiation. As a result, there are no artifacts of reflections within the spatial Nyquist frequency in Fig. 9(b-2) and a localized sound zone was generated even in a reverberant environment. However, the results of Figs. 9(b-1) and (b-2) suggest that the higher the temporal frequency of the sound produced f, the more artifacts occur beyond the spatial Nyquist frequency.

Although the results of Figs. 9(b-1) and (b-2) use a spherical array of 162 loudspeakers with $r_0 = 0.25$ m, the spatial Nyquist frequency is only about 2.1 kHz and no listener can be in the space because the size of the array is too small. This fact also suggests that *ERC-SP* requires a huge number of loudspeakers for its practical implementation.

Compared with *ERC-SP*, the sound pressure is slightly propagated at $r > r_0$ in the results of *ERC-CL* as shown in Figs. 7(d-1) and (d-2), 8(c-1) to (d-2) and 9(c-1) to (d-2). This is because (38) suggests that *ERC-CL* can only cancel out the propagation wave components radiated from a circular array at $r > r_0$ and the evanescent components are radiated at $r > r_0$. The evanescent wave components radiate about one wave length corresponding to the temporal frequency [22] which can be seen in Figs. 9(c-1) to (d-2). From Figs. 9(c-1) to (d-2), the spatial Nyquist frequency in Figs. 9(c-1) to (d-2) is about 3.4 kHz and *ERC-CL* cannot control the sound field beyond the Nyquist frequency.

ERC-CL uses a truncated linear array of loudspeakers and the truncation error cannot be ignored and the external radiation cannot be cancelled around the edges of a linear array when the radius of a circular array is large. Figs. 8(c-1) to (d-2) show that the accuracy of cancelation of the external radiation was worse and artifacts of reflections were observed when the radius of a circular array was large.

Although *ERC-SP* introduces a surrounding spherical array within which is difficult for listeners to be, in *ERC-CL*, listeners can be in the control area at $r < r_0$ without

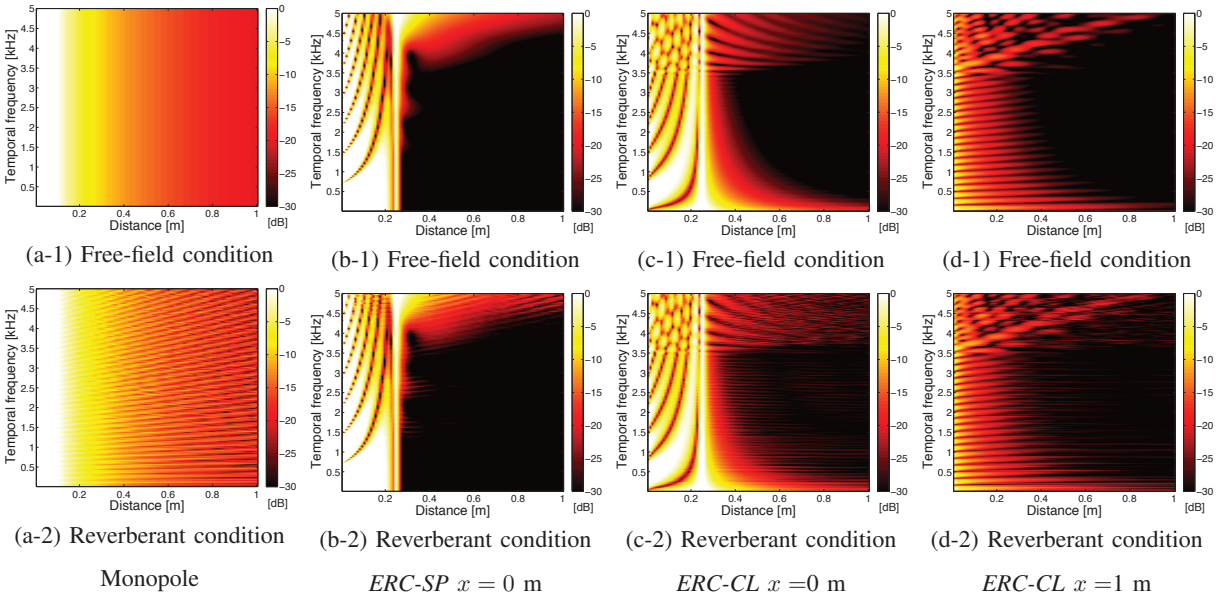

FIGURE 9. Results of sound pressure level $20\log_{10}|P(\boldsymbol{x},\omega)|$ produced by (a) monopole point source, (b) *ERC-SP* with $N_{\mathrm{S}} = 162$ and $R_0 = 0.25$ m, (c)-(d) *ERC-CL* with $N_{\mathrm{C}} = 32$, $N_{\mathrm{L}} = 64$, $r_0 = 0.25$ m and $\Delta x = 0.05$ m for $f = 0.01$ to 5 kHz, $0.1 \leq y \leq 1$ m and $z = 0$ m in (1) the free-field condition and (2) the reverberant condition. Sound pressure level at $\boldsymbol{x} = [0,\ 0.1,\ 0]^{\mathrm{T}}$ for $f = 1$ kHz is set to 0 dB.

$x = 0$. The results of Figs. 9(d-1) and (d-2) suggest that *ERC-CL* can effectively generate a localized sound area on $x = 1$ in both the free-field and reverberant environments. As a result, *ERC-CL* can generate a larger localized sound area with fewer loudspeakers and is more suited for actual implementations than *ERC-SP*. Therefore, there is a trade-off between *ERC-SP* and *ERC-CL*. The theoretical performance of *ERC-SP* is higher than for *ERC-CL* but *ERC-CL* is more suited to actual implementation than *ERC-SP*.

An example of *ERC-CL* implementation combined with large displays is depicted in Fig. 10. According to the simulation results of *ERC-CL*, each *ERC-CL* system with 96 loudspeakers whose length is about 3.2 m mounted above users can provide different audio-visual contents to different users without headphones in a reverberant environment up to $f = 3.5$ kHz which almost covers telephone speech quality. These loudspeaker arrays and control systems can be implemented by actual consumer products. This application is therefore expected to activate multimedia technology since it has never been realized by conventional multiple sound zone generation approaches.

Finally, the extended work for actual implementation are discussed. Spatio-temporal forbidden frequencies discussed in Sec. 3.3 are observed in Figs. 7(d-1), (d-2), 8(b-1) to (d-2) and 9(b-1) to (d-2) as dips within $R < R_0$ and $r < r_0$. To solve this problem, extended approaches, such as introducing another spherical or circular array with different radius [44] as applied to an open spherical microphone array [45], are required as future work. Although loudspeakers are assumed as omni-directional monopole sources in the proposed methods, loudspeakers in actual environments are directional and not point sources. Therefore, the proposed method should be extended to be suitable when using such loudspeakers.

6. **Conclusions.** This paper proposed two effective localized sound zone generation methods based on external radiation cancelling for personal sound systems. The basic concept

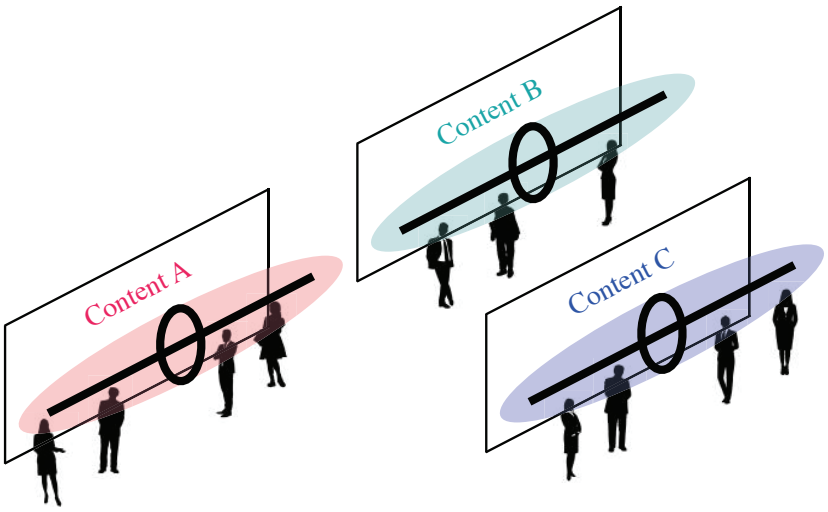

FIGURE 10. An example of *ERC-CL* implementation combined with large displays.

of the proposed methods is that the sound pressure produced by a spherical or a circular loudspeaker array outside the sphere or circle is perfectly cancelled out using another point source or linear loudspeaker array.

The radiation properties of linear, circular and spherical secondary monopole source distributions were analytically derived. These formulations showed that the radiation properties of a spherical or circular sound source outside the sphere or circle are different from those inside them. From these properties, two localized sound zone generation methods, one using a spherical loudspeaker array and a point source named *ERC-SP* and the other using a circular and linear loudspeaker array combination named *ERC-CL* were proposed. The driving signals and radiated sound pressures of both methods were analytically derived.

The most important impact of this paper was that both proposed methods can generate three-dimensional localized sound zones, in both a free-field condition and a reverberant environment, by complete external radiation cancelling, whereas most previous studies have taken only a two-dimensional sound field or free-field condition into account. This impact was shown using analytically derived formulations and the results of the computer simulations for both free-field and reverberant conditions. Moreover, the proposed methods were compared using both formulations and results from computer simulations. These comparisons suggested that there is a trade-off between them: The theoretical performance of *ERC-SP* is better than *ERC-CL* but *ERC-CL* was more suited for actual implementations than *ERC-SP*. An example of *ERC-CL* implementation combined with large displays was presented and it is expected to advance multimedia technology.

Acknowledgment. This study was partly supported by JSPS KAKENHI Grant Numbers 25871208 and 15K21674.

Appendix: Inverse Fourier transform of 0-th order Bessel function. From the inverse transform of the following relationships (3.876-1) [36]:

$$\int_0^\infty \frac{\sin(p\sqrt{x^2+a^2})}{\sqrt{x^2+a^2}} \cos bx dx = \begin{cases} \frac{\pi}{2} J_0\left(a\sqrt{p^2+b^2}\right) & \text{for } 0 < b < p \\ 0 & \text{for } 0 < b < p \end{cases}, \tag{40}$$

where $a > 0$, and the inverse Fourier transform of the 0-th order Bessel function can be analytically derived as:

$$\frac{1}{2\pi}\int_{-\infty}^{\infty} J_0(r_0\sqrt{k^2-k_x^2})e^{-jk_x x}dk_x = \frac{1}{\pi}\cdot\frac{\sin(k\sqrt{x^2+r_0^2})}{\sqrt{x^2+r_0^2}} \quad \text{for} \quad |k| > |k_x|. \tag{41}$$

REFERENCES

[1] W. F. Druyvesteyn and J. Garas, "Personal sound," *J. Audio Eng. Soc.*, vol. 45, no. 9, pp. 685–701, Sept. 1997.

[2] J.-H. Chang, C.-H. Lee, J.-Y. Park, and Y.-H. Kim, "A realization of sound focused personal audio system using acoustic contrast control," *J. Acoust. Soc. Am.*, vol. 125, no. 4, pp. 2091–2097, Apr. 2009.

[3] S. J. Elliott, J. Cheer, J.-W. Choi, and Y. Kim, "Robustness and regularization of personal audio systems," *IEEE Trans. Audio, Speech, Lang. Process.*, vol. 20, no. 7, pp. 2123–2133, Sept. 2012.

[4] Y. Cai, M. Wu, and J. Yang, "Sound reproduction in personal audio systems using the least-squares approach with acoustic contrast control constraint," *J. Acoust. Soc. Am.*, vol. 135, no. 2, pp. 734–741, Feb. 2014.

[5] P. Coleman, P. J. B. Jackson, M. Olik, and J. A. Pedersen, "Personal audio with a planar bright zone," *J. Acoust. Soc. Am.*, vol. 136, no. 4, pp. 1725–1735, Oct. 2014.

[6] M. A. Poletti and F. M. Fazi, "An approach to generating two zones of silence with application to personal sound systems," *J. Acoust. Soc. Am.*, vol. 137, no. 2, pp. 598–605, Feb. 2015.

[7] T. Betlehem, W. Zhang, M. Poletti, and T. Abhayapala, "Personal sound zones: Delivering interface-free audio to multiple listeners," *IEEE Signal Process. Mag.*, vol. 32, no. 2, pp. 81–91, Mar. 2015.

[8] M. A. Poletti and F. M. Fazi, "Generation of half-space sound fields with application to personal sound systems," *J. Acoust. Soc. Am.*, vol. 139, no. 3, pp. 1294–1302, Mar. 2016.

[9] T. Okamoto, "Generation of multiple sound zones by spatial filtering in wavenumber domain using a linear array of loudspeakers," in *Proc. ICASSP*, May 2014, pp. 4733–4737.

[10] T. Okamoto, "Analytical methods of generating multiple sound zones for open and baffled circular loudspeaker arrays," in *Proc. WASPAA*, Oct. 2015.

[11] T. Okamoto and A. Sakaguchi, "Experimental validation of spatial Fourier transform-based multiple sound zone generation with a linear loudspeaker array," *J. Acoust. Soc. Am.*, vol. 141, no. 3, pp. 1769–1780, Mar. 2017.

[12] J.-W. Choi and Y.-H. Kim, "Generation of an acoustically bright zone with an illuminated region using multiple sources," *J. Acoust. Soc. Am.*, vol. 111, no. 4, pp. 1695–1700, Apr. 2002.

[13] M. Shin, S. Q. Lee, F. M. Fazi, P. A. Nelson, D. Kim, S. Wang, K. H. Park, and J. Seo, "Maximization of acoustic energy difference between two spaces," *J. Acoust. Soc. Am.*, vol. 128, no. 1, pp. 121–131, July 2010.

[14] P. Coleman, P. J. B. Jackson, M. Olik, M. Møller, M. Olsen, and J. A. Pedersen, "Acoustic contrast, planarity and robustness of sound zone methods using a circular loudspeaker array," *J. Acoust. Soc. Am.*, vol. 135, no. 4, pp. 1929–1940, Apr. 2014.

[15] M. Shin, F. M. Fazi, P. A. Nelson, and F. C. Hirono, "Controlled sound field with a dual layer loudspeaker array," *J. Sound Vib.*, vol. 333, no. 16, pp. 3794–3817, Aug. 2014.

[16] Y. J. Wu and T. D. Abhayapala, "Spatial multizone soundfield reproduction: Theory and design," *IEEE Trans. Audio, Speech, Lang. Process.*, vol. 19, no. 6, pp. 1711–1720, Aug. 2011.

[17] N. Radmanesh and I. S. Burnett, "Generation of isolated wideband sound fields using a combined two-stage lasso-ls algorithm," *IEEE Trans. Audio, Speech, Lang. Process.*, vol. 21, no. 2, pp. 378–387, Feb. 2013.

[18] W. Jin and W. B. Kleijn, "Theory and design of multizone soundfield reproduction using sparse methods," *IEEE/ACM Trans. Audio, Speech, Lang. Process.*, vol. 23, no. 12, pp. 2343–2355, Dec. 2015.

[19] N. Radmanesh, I. S. Burnett, and B. D. Rao, "A Lasso-LS optimization with a frequency variable dictionary in a multizone sound system," *IEEE/ACM Trans. Audio, Speech, Lang. Process.*, vol. 24, no. 3, pp. 583–593, Mar. 2016.

[20] W. Zhang, T. D. Abhayapala, T. Betlehem, and F. M. Fazi, "Analysis and control of multi-zone sound field reproduction using modal-domain approach," *J. Acoust. Soc. Am.*, vol. 140, no. 3, pp. 2134–2144, Sept. 2016.

[21] T. Okamoto, S. Enomoto, and R. Nishimura, "Least squares approach in wavenumber domain for sound field recording and reproduction using multiple parallel linear arrays," *Appl. Acoust.*, vol. 86, pp. 95–103, Dec. 2014.
[22] E. G. Williams, *Fourier Acoustics: Sound Radiation and Nearfield Acoustic Holography.* San Diego: Academic Press, 1999.
[23] H. Itou, K. Furuya, and Y. Haneda, "Evanescent wave reproduction using linear array of loudspeakers," in *Proc. WASPAA*, Oct. 2011, pp. 37–40.
[24] H. Itou, K. Furuya, and Y. Haneda, "Localized sound reproduction using circular loudspeaker array based on acoustic evanescent wave," in *Proc. ICASSP*, Mar. 2012, pp. 221–224.
[25] J.-H. Chang and F. Jacobsen, "Sound field control with a circular double-layer array of loudspeaker," *J. Acoust. Soc. Am.*, vol. 131, no. 6, pp. 4518–4525, June 2012.
[26] J.-H. Chang and F. Jacobsen, "Experimental validation of sound field control with a circular double-layer array of loudspeakers," *J. Acoust. Soc. Am.*, vol. 133, no. 4, pp. 2046–2054, Apr. 2013.
[27] W. A. Veronesi and J. D. Maynard, "Digital holographic reconstruction of sources with arbitrarily shaped surfaces," *J. Acoust. Soc. Am.*, vol. 85, no. 2, pp. 588–598, Feb. 1989.
[28] T. Okamoto, "Analytical approach to 2.5D sound field control using a circular double-layer array of fixed-directivity loudspeakers," *Proc. ICASSP*, Mar. 2017, pp. 91–95.
[29] T. Okamoto, "Horizontal local sound field propagation based on sound source dimension mismatch," *J. Inf. Hiding Multimed. Signal Process.*, vol. 8, no. 5, pp. 1609–1081, Sept. 2017.
[30] M. A. Poletti, F. M. Fazi, and P. A. Nelson, "Sound reproduction systems using variable-directivity loudspeakers," *J. Acoust. Soc. Am.*, vol. 129, no. 3, pp. 1429–1438, Mar. 2011.
[31] J.-W. Choi and Y.-H. Kim, "Sound field reproduction of a virtual source inside a loudspeaker array with minimal external radiation," *IEEE Trans. Audio, Speech, Lang. Process.*, vol. 21, no. 2, pp. 247–259, Feb. 2013.
[32] B. Rafaely, "Spherical loudspeaker array for local active control of sound," *J. Acoust. Soc. Am.*, vol. 125, no. 5, pp. 3006–3017, May 2009.
[33] T. Okamoto, "Near-field sound propagation based on a circular and linear array combination," in *Proc. ICASSP*, Apr. 2015.
[34] M. A. Poletti, "Three-dimensional surround sound systems based on spherical harmonics," *J. Audio Eng. Soc.*, vol. 53, no. 11, pp. 1004–1025, Nov. 2005.
[35] B. Rafaely, "Spherical loudspeaker array for local active control of sound," *J. Acoust. Soc. Am.*, vol. 125, no. 5, pp. 3006–3017, May 2009.
[36] I. S. Gradshteyn and I. M. Ryzhik, *Table of Integrals, Series, and Products.* New York: Academic Press, 2007.
[37] J. Ahrens and S. Spors, "Sound field reproduction using planar and linear arrays of loudspeakers," *IEEE Trans. Audio, Speech, Lang. Process.*, vol. 18, no. 8, pp. 2038–2050, Nov. 2010.
[38] F. Schultz and S. Spors, "Comparing approaches to the spherical and planar single layer potentials for interior sound field synthesis," *Acta Acust. Acust.*, vol. 100, no. 5, pp. 900–911, Sept. 2014.
[39] Y. Haneda, K. Furuya, S. Koyama, and K. Niwa, "Close-talking spherical microphone array using sound pressure interpolation based on spherical harmonic expansion," in *Proc. ICASSP*, May 2014, pp. 604–608.
[40] T. Okamoto, "2.5D higher-order Ambisonics for a sound field described by angular spectrum coefficients," *Proc. ICASSP*, Mar. 2016, pp. 326–330.
[41] T. Okamoto, "Angular spectrum decomposition-based 2.5D higher-order spherical harmonic sound field synthesis with a linear loudspeaker array," *Proc. WASPAA*, Oct. 2017, pp. 180–184.
[42] A. H. Nasri, "Polyhedral subdivision methods for free-form surfaces," *ACM Trans. Graph.*, vol. 6, no. 1, pp. 29–73, Jan. 1987.
[43] J. B. Allen and D. A. Berkley, "Image method for efficiently simulating small-room acoustics," *J. Acoust. Soc. Am.*, vol. 65, no. 4, pp. 943–950, Apr. 1979.
[44] F. M. Fazi and P. A. Nelson, "Nonuniqueness of the solution of the sound field reproduction problem with boundary pressure control," *Acta Acust. Acust.*, vol. 98, no. 1, pp. 1–14, Jan. 2012.
[45] I. Balmages and B. Rafaely, "Open-sphere designs for spherical microphone arrays," *IEEE Trans. Audio, Speech, Lang. Process.*, vol. 15, no. 2, pp. 727–732, Feb. 2007.